

Figure 3a, b. The shock waves over a flat plate with a sharp leading edge inclined at (a) 5° and (b) 6° to the flow direction inside the test section of the HST1 tunnel at Mach number 5.75.

The experiments were conducted with the following test conditions: flow Mach number = 5.75, Reynolds number = $1 \times 10^5 \text{ m}^{-1}$, freestream density = $1 \times 10^{-2} \text{ kg/m}^3$, duration of the steady flow ~800 μs , freestream temperature = 173 K and freestream static pressure = $9.9 \times 10^{-3} \text{ mbar}$. In these experiments the point electrode was used as the anode and the line electrode was used as cathode. The voltage applied across the electrodes was about 1500 V and the electric current was set at 1 A. The discharge in the test section was photographed from outside the side window using a Nikon FM 2.8 camera with B exposure. A film with ASA 1600 speed was used for recording the weak light emitted from the discharge field. Some of the photographs were taken at film speeds of ASA 3200 and ASA 6400 by using the push processing technique in order to record the spectral variation of the light emitted from the temperature layer. However these preliminary experiments did not reveal the temperature layer because the temperature in this layer will be very low for the flat plate with a sharp lead-

ing edge. Currently the efforts are being made to study the temperature layer with a blunt nose cone model.

Typical results of the shock shape visualization are shown in Figure 3a and b for the flat plate at 5 and 6 degrees angle of attack, respectively. Unlike the dark line representing the position of the shock wave in the long-duration tunnels¹, the shock position in these figures is indicated by the bright line. The bright portion at the shock wave occurs in this case because the experimental conditions are suitable to make the electron energy at the shock wave equal to about 20 eV (ref. 3). The measured shock wave angles of 13° and 14° match very well with those theoretically estimated using oblique shock relationship⁴ for both the cases.

In conclusion, we have demonstrated a new technique for the visualization of the shock shapes around the hypersonic vehicles tested in hypersonic shock tunnel. This method is novel as it suits application in the shock tunnel where the typical test times are less than a millisecond. The measured shock angles for a flat plate with sharp leading edge at an angle of attack tested at flow Mach number 5.75 in IISc shock tunnel HST1 match very well with the theoretical results. This technique can be utilized for visualizing the three-dimensional shock shapes by taking the photograph of the electrical discharge either in the downstream or upstream direction of the flow.

1. Nishio, M., *AIAA J.*, 1990, 28, 2085–2091.
2. Nasser, E., *Fundamentals of Gaseous Ionization and Plasma Electronics*, Wiley Interscience, New York, 1970.
3. Nishio, M. and Itho, H., *Trans. Jpn. Soc. Aero. Space Sci.*, 1995, 38, 38–45.
4. Anderson, Jr., J. D., *Hypersonic and High Temperature Gas Dynamics*, McGraw-Hill, New York, 1989.

Received 13 June 1996; accepted 2 July 1996.

Steric enhancement of resonance: An electron localization perspective

Shridhar R. Gadre, Libero J. Bartolotti* and C. H. Suresh

Department of Chemistry, University of Pune, Pune 411 007, India

*North Carolina Supercomputing Center, 3021 Cornwallis Road, Research Triangle Park, NC 27709, USA

Steric enhancement of resonance (SER) has earlier been characterized in terms of molecular properties such as dipole moment, bathochromic shift, mesomeric moment, spin-spin coupling constant or by monitoring the kinetics of a reaction. The present work provides a unified picture of SER in terms of the electron localization patterns in a molecule.

THE phenomenon of steric hindrance of resonance (SHR) has been well documented¹ in the organic chem-

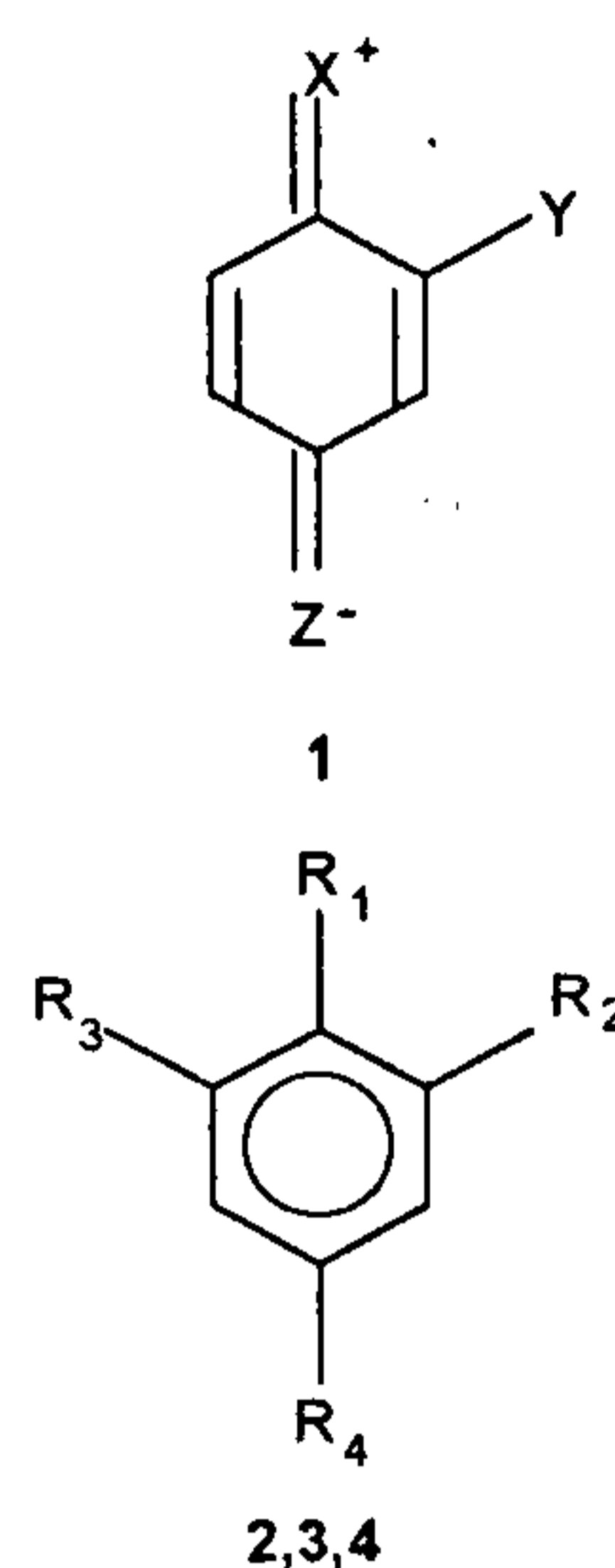
istry literature for a long time. However, that of steric enhancement of resonance (SER) has been discussed²⁻⁸ rather scantily and only for the past three decades or so. SER was first noticed by Baliah and Uma² during their dipole moment measurements of some substituted anisoles. Later, Kamlet *et al.*^{3,4} invoked the same phenomenon for explaining bathochromic shifts observed in the absorption spectra of some alkylnitrobenzenes and substituted 2,4-dinitroanilines. Similarly, the higher rates of solvolysis (4 times) shown by 3-methyl 4-methoxy benzylchloride, as compared to 4-methoxy benzylchloride have been explained in terms of the SER phenomenon⁵. Some other physical data in the literature supporting this phenomenon are: the calculated and observed dipole moment values for 2,4-dinitroanisole and 1-methoxy-2,4-dinitronaphthalene⁶, the spin-spin coupling constants between the methyl protons and the ortho ring protons of a number of substituted anisoles⁷ and the ¹⁶O and ¹³C NMR chemical shifts of 2-substituted, 2,6-disubstituted and 2,4,6-trinitroanisol⁸. In the above-mentioned works, SER manifests in many diverse ways. The question addressed in the present communication is: can one obtain a common electronic signature for these wide-ranging physico-chemical observances regarding SER?

The recent works done by Gadre *et al.*⁹⁻¹³ have demonstrated that MESP topography is a convenient tool for monitoring the subtle changes in electronic distribution in molecules. The MESP, $V(\mathbf{r})$, at a point \mathbf{r} due to a molecular system with nuclear charges $\{Z_A\}$ located at $\{\mathbf{R}_A\}$ and electron density $\rho(\mathbf{r})$ is given by

$$V(\mathbf{r}) = \sum_A^N Z_A / |\mathbf{r} - \mathbf{R}_A| - \int \rho(\mathbf{r}') d^3\mathbf{r}' / |\mathbf{r} - \mathbf{r}'|,$$

where N is the total number of nuclei in the molecule. The terms on the rhs of the above equation represent the nuclear contribution and the electronic contributions respectively. When the electronic factor overrides the nuclear one, $V(\mathbf{r})$ becomes negative and a large negative value for it physically implies a higher electron localization around that point. These points of maximum electron localizations or minimum MESP value can be rigorously characterized by the topological analysis⁹⁻¹³ of MESP based on the identification and location of its minima.

In general SER phenomenon can occur in two ways^{4,5}. In the first case, it may occur in a system such as **1** where, X is a $+R$ or $+I$ substituent and Y and Z are $-R$ substituents⁴. It follows that progressively increasing the bulk of X forces Y from out of the ring plane, and this leads to a decrease in the power of Y to withdraw electrons from the ring and X . This is the classical situation of SHR. A counter-effect of this leads to the enhancement of the resonance interaction between X and Z and is termed as SER⁴. The second situation is observed in



	R ₁	R ₂	R ₃	R ₄
2a	H	H	H	CH ₂ Cl
2b	H	H	CH ₃	CH ₂ Cl
2c	OCH ₃	H	H	CH ₂ Cl
2d	OCH ₃	CH ₃	H	CH ₂ Cl
2e	OCH ₃	CH ₃	CH ₃	CH ₂ Cl
3a	OCH ₃	H	H	H
3b	OCH ₃	CH ₃	H	H
3c	OCH ₃	CH ₃	CH ₃	H
4a	NH ₂	NO ₂	H	H
4b	NH(CH ₃)	NO ₂	H	H
4c	N(CH ₃) ₂	NO ₂	H	H

Figure 1.

substituted anisoles or thioanisoles^{2,5}. When a substituent is present ortho to the methoxyl group, the free rotation of the $-OCH_3$ group is restricted and it takes a preferred orientation that is anti to the 2-substituent and coplanar to the ring plane. This geometry enables the methoxyl group to conjugate more effectively with the group at the 4-position.

We have explored **2**, **3** and **4** (Figure 1) as test examples towards an appraisal of SER in terms of features of electron distribution. Our earlier MESP topographical analysis of substituted benzenes¹² demonstrated that the orientation effect as well as the activation or deactivation exhibited by the substituents can be very well represented by the position and the values of the MESP minimum. It was also found that using a molecular geometry optimized at a lower basis-set (typically 6-31 G) and a wave function obtained at a higher basis-set (usually 6-31 G**) is generally quite sufficient for an adequate topological representation of MESP. All the molecules reported in this work are fully optimized at HF/6-31G level using GAUSSIAN94 (ref. 14) package. Using these geometries, the wave function at HF/6-31 G** level is calculated and employed for the MESP topographical analysis. Packages UNIPROP (ref. 15) and UNIVIS (ref. 16) developed in our laboratory are employed for this purpose.

In all the substituted benzylchlorides **2a-e**, the plane which contains the chlorine, the benzyl carbon and a ring carbon is perpendicular to the ring plane. When both the ortho-positions of $-OCH_3$ are occupied by $-CH_3$ group **2e** and **3c**, the plane defined by the methoxyl carbon, oxygen and a ring carbon makes an angle 90° , which otherwise makes an angle of 0° with respect to the benzene ring. The methoxyl group and the chlorine atom are seen on the same side of the ring in

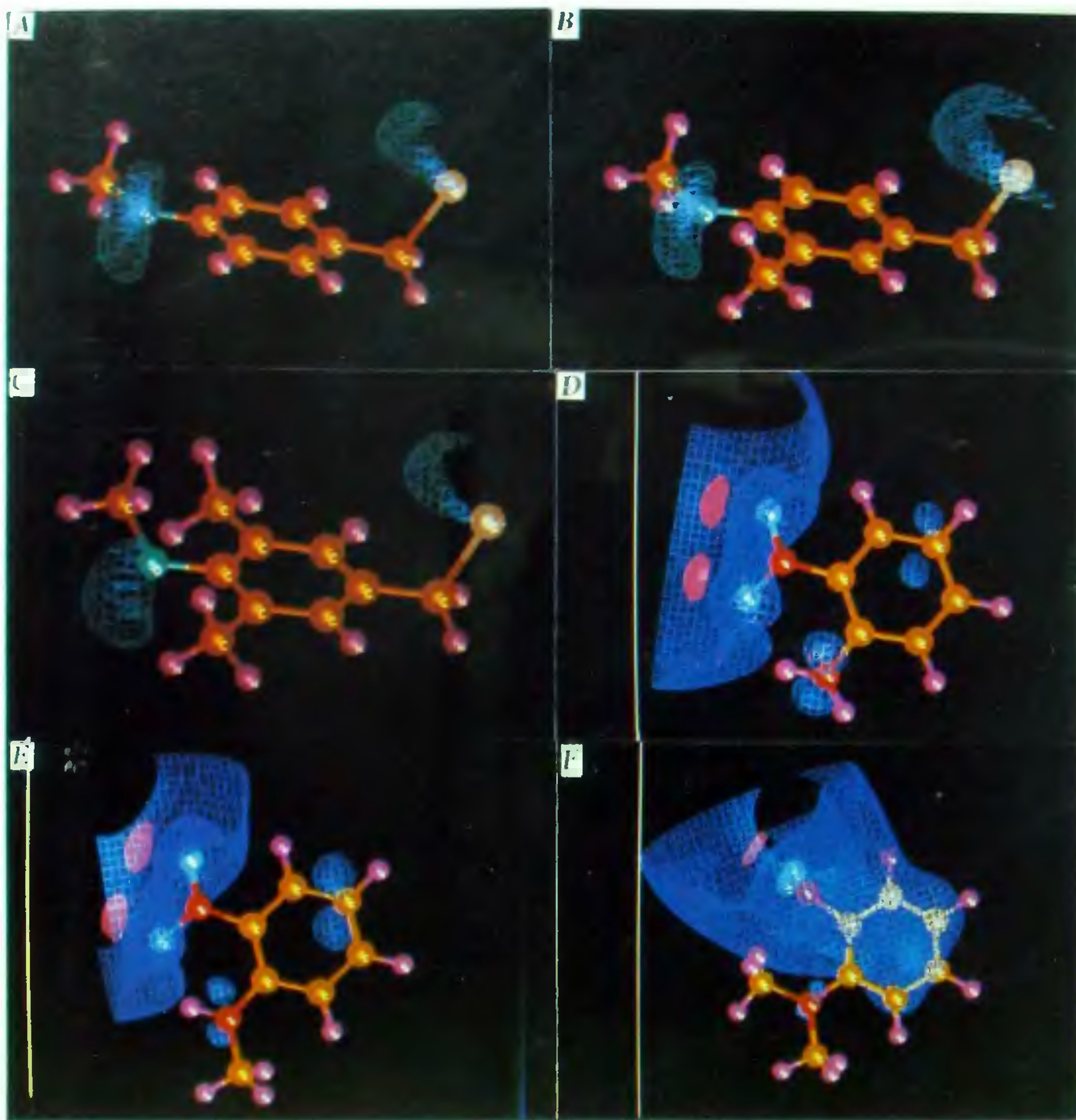


Figure 2 A–C. MESP iso-surface corresponding to $-115.41 \text{ kJ mol}^{-1}$ for systems 2c, 2d and 2e respectively; D–F, MESP iso-surface corresponding to $-31.48 \text{ kJ mol}^{-1}$ (blue surfaces) and $-194.10 \text{ kJ mol}^{-1}$ (red surfaces) for systems 4a, 4b and 4c respectively.

3,5-dimethyl 4-methoxybenzylchloride, 2a. In 2-nitroanilines 4a–c, except the case of 4c all the heavy atoms

are lying in the benzene ring plane. In 4c, the nitro group is not in the ring plane, but exactly perpendicular to it.

Table 1. MESP minima for systems **2**, **3** and **4**. All values are in kJ mol^{-1}

Structure	Oxygen minimum	Chlorine minimum	Para carbon (with respect to $-\text{OCH}_3$ or $-\text{NR}_2$) minimum	Nitrogen minimum
2c	-176.79	-124.07	-	-
2d	-171.28	-132.72	-	-
2e	-199.87	-125.38	-	-
3a	-200.13	-	-89.97	-
3b	-195.98	-	-96.00	-
3c	-212.46	-	-87.61	-
4a	-228.46	-	-36.20	-57.44
4b	-230.82	-	-39.61	-44.59
4c	-206.69	-	-52.46	-41.97

In benzene, the MESP minimum for the π -cloud is -85.5095 (all values quoted here are in kJ mol^{-1}). The substitution of one hydrogen by the $-\text{CH}_2\text{Cl}$ group, **2a**, deactivates the ring and the MESP value of the ring minimum is increased to -51.41 . The chlorine MESP minimum is -121.71 in **2a**, which in the case of methyl chloride is -94.43 , indicating that the electron density around the chlorine atom is enhanced at the expense of the ring π -electron density. The electron flow towards the chlorine is further increased when one electron donating group is introduced in the aromatic ring. A methyl group at the meta position **2b** or a methoxyl group at the para position **2c** changes the minimum ESP of chlorine to -124.07 and -129.31 , respectively. When both are present, **2d**, the MESP minimum of chlorine goes down to -132.72 , i.e. a decrease by 11.02 units, which is a little higher than the added effect of the $-\text{CH}_3$ and $-\text{OCH}_3$ groups. By adding one more methyl group at the remaining ortho position of $-\text{OCH}_3$ group, **2e**, the value of the chlorine minimum goes deeper by 3.67 than the chlorine minimum of **2a**. Exactly complementary trend in the values of the oxygen MESP minimum is observed in **2c**, **2d** and **2e** (see Table 1). Oxygen minimum is less negative in **2d** compared to **2c** and it is more negative in **2e**. A decrease in the magnitude of oxygen MESP minimum is compensated by an increase in the magnitude chlorine minimum (Table 1). This feature is graphically brought out by Figure 2, wherein iso-surface of MESP with value of -115.4116 is depicted for **2c**, **2d**, and **2e** in Figure 2A, B and C respectively. The lobe of iso-surface with value -115.41 is the largest in Figure 2C for **2e** at the expense of the chlorine lone-pair. The lobe is the largest in Figure 2B for **2d**.

The changes seen in the chlorine minimum can be correlated to the kinetic data on the solvolysis of systems **2a–e** reported by Baliah and Kanagasabapathy⁵. They have explained the unusually higher rate of reaction of system **2d** and the unusually lower reactivity of **2e** by invoking the concept of SER. In their opinion, a sub-

stituent ortho to methoxyl group does not sterically inhibit the methoxyl group from conjugating with the benzene ring, but makes the conjugation more effective than in the absence of the ortho substituent. In the present context, the observation of a highly negative valued chlorine minimum in **2d** supports their argument and it points out that such a minimum may make the leaving process of Cl^- easier and accounts for the higher rate of solvolysis of **2d**. When both ortho positions are occupied, **2e**, the methoxyl group prefers a perpendicular orientation with respect to the benzene ring and this makes the conjugation of the oxygen lone pairs with the benzene ring difficult, hence the $-I$ effect of oxygen decides the electron distribution.

In the absence of the electron withdrawing group $-\text{CH}_2\text{Cl}$, viz. in systems **3a**, **3b** and **3c**, a MESP minimum appears above the para carbon atom with respect to the methoxyl group. A comparison of the values of the para minimum and the oxygen minimum (Table 1) once again confirms the SER phenomenon.

In 2-nitroanilines **4a–c** the interplay of the steric and the electronic effects can be monitored using three different MESP minima. Here we report one of the $-\text{NO}_2$ oxygen minimum, one minimum seen above the para carbon and the $-\text{NR}_2$ nitrogen minimum (Table 1). Going from **4a** to **4b**, the oxygen minimum as well as the carbon minimum becomes more negative (the change is 2.36 and 3.41 respectively) due to the more electron push from the $-\text{NH}(\text{CH}_3)$ group compared to the $-\text{NH}_2$ group. At the same time the nitrogen minimum goes up by 12.85. When the substituent is $-\text{N}(\text{CH}_3)_2$ the $-\text{NO}_2$ group goes completely out of the ring plane and this leads to a significant increase in the oxygen MESP minimum (an increase by 21.77 with respect to **4a**), visually seen in Figure 2. This explains the classical situation of SHR. A deepening of the para carbon minimum by 16.26 shows the counter effect of this phenomenon, the SER. This effect can be visually seen in Figure 2D, E and F in terms of MESP iso-surfaces with values of -31.48 and -194.10 . This enhancement is due to the more electron donation from the donor as well as the diminished electron-pulling effect of the acceptor.

The above observations on the substituted benzylchlorides and substituted anisoles lead us to the following important conclusions. There is indeed a unique electronic signature of the steric enhancement of resonance phenomenon. The phenomenon can be monitored by the electron concentration patterns through the MESP topography.

1. See, for example, March J., *Advanced Organic Chemistry: Reactions, Mechanisms and Structure*, Wiley Eastern, New Delhi, 1992, p. 34 and 471.
2. Baliah, V. and Uma, M., *Tetrahedron Lett.*, 1960, **25**, 21–25.
3. Kamlet, M. J., Hoffsommer, J. C. and Adolph, H. C., *J. Am. Chem. Soc.*, 1962, **84**, 3925–3928.

4. Kamlet, M. J., Adolph, H. C. and Hoffsommer, J. C., *J. Am. Chem. Soc.*, 1964, 86, 4018-4021.
5. Baliah, V. and Kanagasabapathy, V. M., *Tetrahedron*, 1978, 34, 3611-3615.
6. Lachmann, P. A. and McEacharm, J. *Mol. Struct.*, 1971, 1, 253.
7. Schuster, I. I., Salmann, S., Wildman, T. A. and Penner, G. H., *Can. J. Chem.*, 1985, 63, 782-786.
8. Schuster, I. I., Parvez, M. and Freyer, A. J., *J. Org. Chem.*, 1988, 59, 5819-5825.
9. Gadre, S. R., Kulkarni, S. A. and Shrivastava, I. H., *J. Chem. Phys.*, 1992, 96, 5253-5260.
10. Shirsat, R. N., Bapat, S. V. and Gadre, S. R., *Chem. Phys. Lett.*, 1992, 200, 373-378.
11. Mehta, G., Gunasekaran, G., Gadre, S. R., Shirsat, R. N., Ganguly, B. and Chandrasekhar, J., *J. Org. Chem.*, 1994, 59, 1953-1955.
12. Mehta, G., Khan, F. M., Gadre, S. R., Shirsat, R. N., Ganguly, B. and Chandrasekhar, J., *Angew. Chem. Int. Ed. Engl.*, 1994, 33, 1390-1391.
13. Gadre, S. R., Kulkarni, S. A., Suresh, C. H. and Shrivastava, I. H., *Chem. Phys. Lett.*, 1995, 239, 273-281.
14. Firsch, M. J., Trucks, G. W., Schlegel, H. B., Gill, P. M. W., Johnson, P. G., Robb, M. A., Cheeseman, J. R., Keith, T. A., Petersson, G. A., Montgomery, J. A., Raghavachari, K., AlLaham, M. A., Zatzewski, V. G., Ortiz, J. V., Foresman, J. B., Cioslowski, J., Stetanov, B. B., Nanayakkara, A., Challacombe, M., Peng, C. Y., Ayala, P. Y., Chen, W., Wong, M. W., Andres, J. L., Replogle, E. S., Gomperts, R., Martin, R. L., Fox, D. J., Binkley, J. S., Defrees, D. J., Baker, J., Stewart, J. P., Head-Gordon, M., Gonzalez, C. and Pople, P. A., *Gaussian 94*, Gaussian Inc., Pittsburgh, PA, 1995.
15. The package UNIPROP developed by Gadre, S. R. and co-workers, Department of Chemistry, University of Pune, Pune, 411 007, India.
16. The package UNIVIS developed by Limaye, A. C., Inamdar, P. V., Dattawadkar, S. M. and Gadre, S. R., *J. Mol. Graph.*, 1996 (in press).

ACKNOWLEDGEMENTS. We thank Professor M. Krishna Pillay for bringing the phenomenon of SER to our notice and for useful discussions. Financial assistance from the CSIR is gratefully acknowledged.

Received 13 May 1996; accepted 20 June 1996

Quantum chaos in Rydberg atoms: A quantum potential approach

P. K. Chattaraj and S. Sengupta

Department of Chemistry, Indian Institute of Technology, Kharagpur 721 302, India

The quantum signature of chaos in Rydberg atoms has been studied using a quantum theory of motion and quantum fluid dynamics. A hydrogen atom in the electronic ground state ($n = 1$) and in an excited electronic state ($n = 20$) behaves differently when placed in an external oscillating electric field. Temporal evolutions of Shannon entropy, density correlation, phase space distance function of Bohmian trajectories and associated Kolmogorov-Sinai entropy for these two cases show marked differences.

CLASSICAL interpretation of quantum mechanics is as old as the quantum mechanics itself. In the Madelung representation¹ the time-dependent Schrödinger equation for a single particle of mass m moving under potential $V(r)$, viz.

$$[-(\hbar^2/2m)\nabla^2 + V(r)]\Psi(r, t) = i\hbar\partial\Psi/\partial t \quad (1)$$

is transformed into two-fluid dynamical equations. Substituting the following polar form of the wave function

$$\Psi(r, t) = R(r, t) \exp(iS(r, t)/\hbar) \quad (2)$$

in eq. (1) and separating the real and the imaginary parts, one obtains an equation of continuity

$$\partial\rho/\partial t + \nabla \cdot j = 0, \quad (3a)$$

and an Euler-type equation of motion

$$\partial v/\partial t + (v \cdot \nabla)v = -(1/m)\nabla(V + V_{qu}). \quad (3b)$$

In eqs (3) the charge density, $\rho(r, t)$ and current density, $j(r, t)$ are

$$\rho(r, t) = [R(r, t)]^2 \quad (4a)$$

and

$$j(r, t) = \rho(r, t)v(r, t). \quad (4b)$$

where the velocity $v(r, t)$ can be defined in terms of the phase of the wave function as

$$v(r, t) = (1/m)\nabla S(r, t). \quad (4c)$$

The quantity V_{qu} appearing in eq. (3b) is called the quantum potential or Bohm potential of hidden variable theory² and defined as

$$V_{qu} = -(\hbar^2/2m)\nabla^2 R/R. \quad (5)$$

Therefore, in this quantum fluid dynamics¹ the overall motion of the system under consideration can be thought of as the motion of a 'probability fluid' having density $\rho(r, t)$ and velocity $v(r, t)$ under the influence of the external classical potential augmented by a quantum potential, V_{qu} .

For the ground state of a many-particle system, $\rho(r, t)$ contains all information³. In a time-dependent situation

This paper is based on a seminar talk delivered by P. K. Chattaraj in the International Discussion Meeting on Time Dependent Quantum Mechanics of Many Electron Systems at Indian Institute of Science, Bangalore in January, 1996.